14th International Symposium on Turbulence and Shear Flow Phenomena (TSFP14)
Heidelberg, Germany, July 28–31, 2026

ON THE IMPACT OF SUPERSTRUCTURES ON THE INSTANTANEOUS WALL-SHEAR STRESS IN ROUGH-WALL BOUNDARY LAYERS

Ioannis K. Kaminaris, Elias Balaras,
Department of Mechanical and Aerospace Engineering
The George Washington University
Washington, DC, USA
kaminaris@gwu.edu; balaras@gwu.edu

Michael P. Schultz
Department of Naval Architecture and Ocean Engineering
United States Naval Academy
Annapolis, MD, USA
mschultz@usna.edu

ABSTRACT

The impact of superstructures on the fluctuating wall-shear stress is investigated in rough-wall spatially developing turbulent boundary layers by means of direct numerical simulations (DNS). A sample of bio-inspired, biofouling-type rough surfaces is utilized in three arrangements all at the same nominal coverage, $\lambda_p \approx 40\%$. The DNS data have been previously validated in Kaminaris *et al.* (2023, 2025*b*). Three-dimensional time-series data are employed to analyze the flow field, as well as to compute the wall-shear stress directly on the surface of the irregular roughness. The wavelengths obtained from the spectral analysis of the wall-shear stress in conjugation with the superstructure length-scales obtained from the cross-correlation of the velocity field unveil that superstructures mainly located in the logarithmic and outer-part of the boundary layer maintain a strong impact on the wall-shear stress that can reach even $\approx 50\%$ of the total spectral energy. Furthermore, it has been found that the roughness impact on the wall-shear stress spectral energy scales with the mean height and that the great majority of the spectral energy comes from the pressure contribution.

Introduction

The presence of roughness is known to significantly alter both the near-wall and outer-layer mean flow structure (see for example Jiménez, 2004; Chung *et al.*, 2021); however little is known on the roughness impact on the flow dynamics. For example, very large scale structures formed in the velocity fluctuation field, also known as superstructures have long been studied in canonical smooth-wall flows. Specifically, Kim & Adrian (1999) reported evidence of very-large coherent motions residing at wall-normal locations even greater than the logarithmic-layer in pipe flows that were detected to extend even up to 14 pipe diameters in length, based on the wavelengths of the streamwise velocity spectra. Such structures have been first identified in smooth-wall boundary layers in Hutchins & Marusic (2007), and they were found to extent up to 20δ in length. Superstructure behavior over *canonical* rough-walls has also been investigated. Wu & Christensen (2010), for example, reported shorter correlation lengths for the superstructures growing over rough-walls when scaled by the local boundary layer thickness. A similar observation was made by Kevin *et al.* (2019) over a surface with converging-diverging riblets, where they estimated their length-scales to be $\approx 4-5\delta$. More recently, the superstructure evolution in turbulent boundary layers over complex non uniform surfaces of biofouling-type was also explored via DNS by Kaminaris *et al.* (2025*a*), where superstructure length-scales were reported in the order of $\approx 2\delta$ in the outer-layer.

Örlü & Schlatter (2011) studied the impact of such structures in the near-wall region and found that the energy spectra of the fluctuating wall-shear stress in inner-coordinates exhibited significant deviation at large wavelengths over a range of different *Re* numbers, highlighting the influence of outer-layer structures at the wall. The superstructure impact on the wall-shear stress was also investigated by Marusic *et al.* (2021), where it was found that the contribution of large-scale motions of the outer-layer to the fluctuating wall-shear stress was significant, ranging from 8% to 30% for $Re_\tau = 10^3$ and $Re_\tau = 10^5$, respectively. The information of the near-wall velocity signal used by Marusic *et al.* (2021) was obtained through a simple mathematical model, proposed in Marusic *et al.* (2010), that predicts the fluctuating near-wall velocity signal based on flow information from the logarithmic region of the boundary layer.

The primary goal of this work is to investigate the degree to which superstructures of the logarithmic- and outer-part of the boundary layer affect the wall-shear stress. To investigate this, biofouling-type surfaces are utilized, while the flow-field is studied via DNS in boundary layer configurations up to $Re_\tau = 3,150$. Pre-multiplied spectra of the fluctuating wall-shear stress are computed and are directly associated with the superstructure characteristic length-scales acquired at various wall-normal locations.

Methodologies and parametric space

The current work employs bio-inspired surfaces of biofouling-type, given their significant importance for the

Topography	Planar solidity λ_p (%)	Frontal solidity λ_f (%)	Mean roughness height $\overline{h}/\delta_{LE}$	Mean organism height $\hbar/\delta_{LE}$	Standard deviation σ/δ_{LE}	Skewness Sk	Kurtosis Ku	Effective Slope ES_{xz}	Roughness Reynolds number k_s^+	Line color
Smooth-wall	-	-	-	-	-	-	-	-	-	green
BS39	39.3	15.9	0.0460	0.090	0.0740	1.409	3.520	0.317	570	red
BR39	39.2	15.5	0.0488	0.097	0.0768	1.311	3.200	0.310	470	blue
TR39	40.1	13.11	0.0209	0.0474	0.0310	1.173	2.826	0.248	105	brown

Table 1 Surface characteristics for the biofouling-type topographies considered in this work.

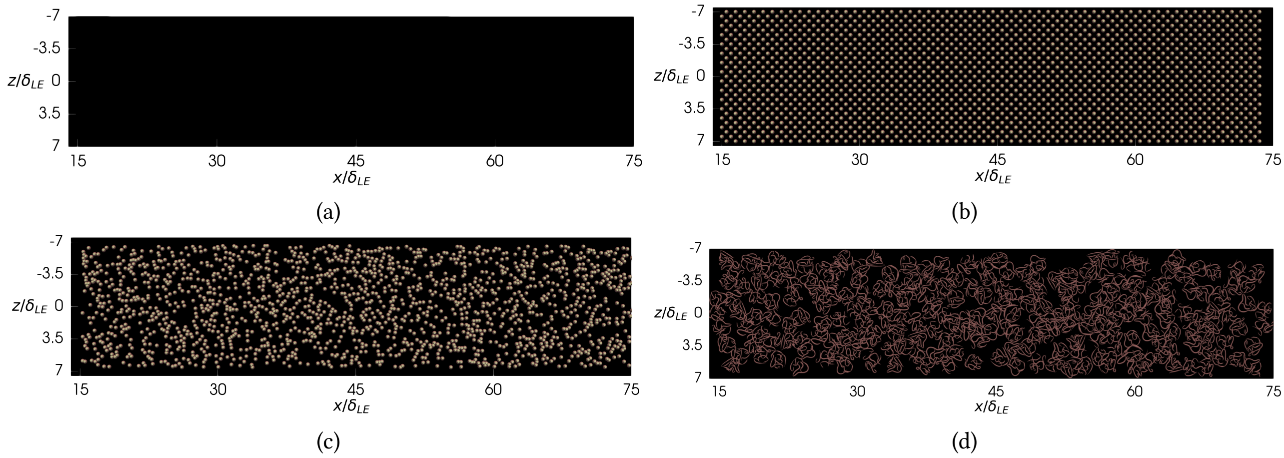

Figure 1: Top view of (a) the smooth-wall and the rough-wall topographies (b) BS39; (c) BR39; (d) TR39.

naval engineering community (see for example Schultz *et al.*, 2011). Specifically, three rough-wall surfaces are considered: one in a staggered arrangement (BS39) comprising only barnacle-type organisms and two in random arrangements comprising i) only barnacle-type (BR39) organisms, ii) only tubeworm-type (TR39) organisms, alongside a reference smooth-wall surface (see Figure 1). The surfaces are designed by our in-house surface synthesis algorithm in order to mimic scans of actual organisms found on ship hulls. All topographies have approximately the same nominal surface coverage, $\lambda_p \approx 40\%$, while the blockage ratio across all surfaces spans a range of $37 \leq \overline{\delta}/\overline{h} \leq 70$ ($\overline{\delta}$ the boundary layer thickness at the middle of the domain). The dimensions of the full computational domain are $100\delta_{LE} \times 14\delta_{LE} \times 10\delta_{LE}$ in the streamwise, spanwise and wall-normal directions, respectively (δ_{LE} the boundary layer thickness at the leading-edge roughness). The computational grid utilized comprised $6002 \times 1202 \times 348$ grid points in the streamwise (x), spanwise (z) and wall-normal (y) directions respectively, which resulted in a resolution of $\Delta x^+ = 10.5$, $\Delta z^+ = 9$ and $\Delta y^+ = 0.9$ (based on the average friction velocity for the smooth part of the plate). The resulting resolution per roughness element in the case of the barnacle-type surfaces is $40 \times 40 \times 70$ points in the streamwise, spanwise and wall-normal directions respectively. For the case of tubeworm-type surfaces, approximately 140 grid points were used to resolve their maximum dimension. The highest friction Reynolds number range obtained within the roughness-patch is $1,700 \leq Re_{\tau,rough} \leq 3,150$, and $750 \leq Re_{\tau,smooth} \leq 1,300$ for the smooth-wall case.

Our in-house, finite-difference, Navier–Stokes solver is utilized for all cases presented in this work. A fractional step method is used for the time advancement where all terms are treated explicitly using the Runge–Kutta third-order scheme. All spatial derivatives are discretised using second-order central-differences on a staggered grid. The code is parallelised using a classical domain decomposition approach. The computational domain is descretized using a Cartesian grid and the roughness elements are represented via a direct-forcing, immersed-boundary method. The details on the overall formulation can be found in Yang & Balaras (2006). The DNS were validated against peer experiments conducted in the US Naval Academy water channel showing very good agreement on both the first and second order statistics (Kaminaris *et al.*, 2023, 2025*b*).

Results

A side view of the superstructures along the boundary layer is shown in Figure 2 visualized via the streamwise fluctuating velocity field. It has been shown through two-point correlations at various wall-normal locations that the superstructure size, $\mathscr{L}/\delta_{LE}$, grows faster under rough-wall conditions compared to smooth-wall, (see Kaminaris *et al.*, 2025*a*). Furthermore, Kaminaris *et al.* (2025*a*) have demonstrated, through volumetric autocorrelations, Proper Orthogonal Decomposition (POD) analysis, as well as visual inspection, that superstructures maintain strong coherence from the boundary layer edge down to the wall. This also holds true in the case of the smooth-wall flows, as discussed by Hutchins & Marusic (2007); Sillero *et al.* (2014).

The near-wall presence of the superstructures can be seen in Figure 3a in a spanwise/wall-normal view for the case of the BR39 topography. To assess their impact on the fluctuating wall-shear stress, τ'_w, spectral analysis with respect to the latter is performed. The computation of the fluctuating wall shear stress, τ'_w, for complex geometries is not trivial and our approach is outlined in Kaminaris *et al.* (2023), where also a detailed validation via comparisons to experiments is included. For all cases included in this work the pressure and viscous wall-shear stress components were acquired are di-

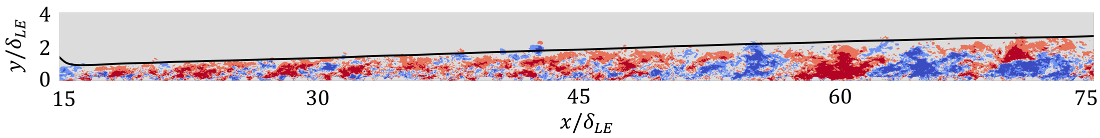

Figure 2: Side view of streamwise velocity fluctuations, u', showing the superstructures on the case of the BR39 surface; The solid black line corresponds to the boundary layer edge.

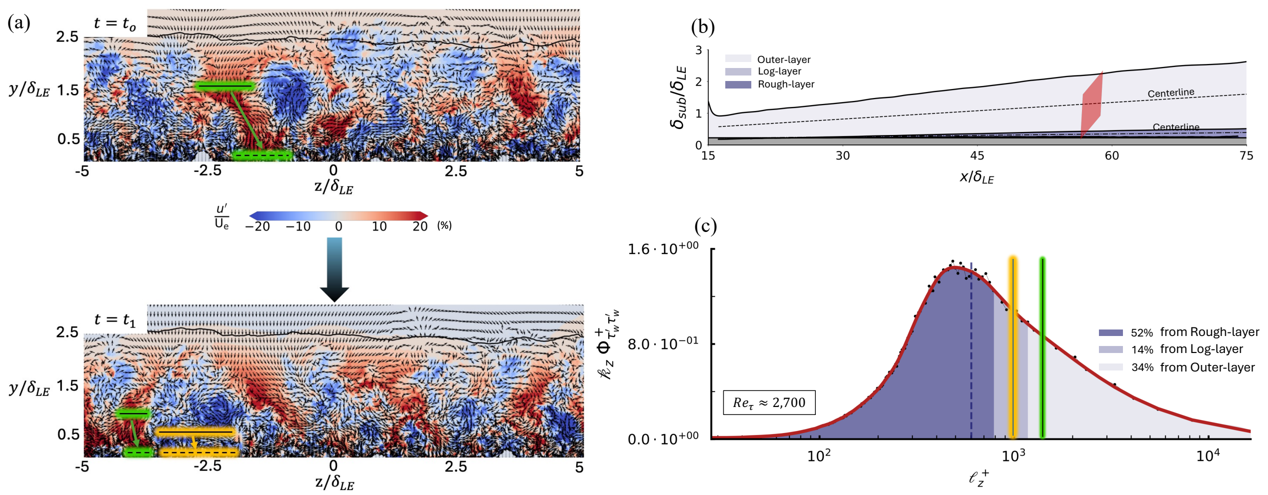

Figure 3: (a) Cross-plane view of the streamwise velocity fluctuations, u', superposed by the cross-plane motions at two distinct instances at the streamwise location of $x/\delta_{LE} = 57.5$; (b) Evolution of the boundary sublayers. Red-plane corresponds to the reference cross-plane; (c) Premultiplied spanwise energy spectra of the fluctuating wall-shear stress, τ'_w in inner-scaling in the case of the BR39 topography at the streamwise location of $x/\delta_{LE} = 57.5$. Color-coded bars and dashed lines indicate the boundary layer part the spectrum wavelengths correspond to in terms of the superstructure widths. Vertical dashed lines correspond to the widths of superstructures at the centerline of each sublayer. Increasing color intensity corresponds to decreasing wall-normal distance. Solid red line corresponds to a low-pass filter of the data.

rectly interpolated onto a uniform Cartesian grid to facilitate processing using Fast Fourier Transform (FFT) algorithms.

The power spectra of τ'_w are computed with respect to the spanwise direction and are averaged in time, as well as in space within a short distance from their nominal streamwise location, to include a larger number of roughness scales and thus to achieve a more accurate energy representation. The power spectra are computed across the spanwise direction, since in this way the former can be mapped to single Reynolds number, contrary to the native streamwise or temporarily-to-streamwise converted spectra where a range of different Reynolds numbers takes place as a result of the streamwise evolving nature of the boundary layer. It should be noted that here the FFT of the wall-shear stress are mapped to the wall-projected surface distance. Thus, the surface curvature along the spanwise direction is not taken into account. This choice is made based on its computational simplicity.

Marusic *et al.* (2021) employed the eddy-turnover time as the demarcation method for the energy cutoff in order to estimate the contribution of outer-layer superstructures on the wall-shear stress and concluded that $\approx 8\%$ of the wall-shear stress energy corresponds to wavelengths as large as those of the superstructures in the outer-layer flow. Here, given that the three-dimensional flow-field is available we take advantage of the estimates made in Kaminaris *et al.* (2025*a*) regarding the superstructure spanwise length-scales, computed at the centerline of each of the main sublayers (shown in Figure 3b), and we use them as demarcation signs for the wavelength-based-energy cutoff. For reference, it is mentioned that all the two-point correlation length-scales are estimated at a cutoff of 0.1. The power spectral density (PSD) of the wall-shear stress demarcated by the superstructure spanwise length-scales can be shown in Figure 3c. Note, that the three main sublayers shown in Figure 3b evolving in space, are estimated through the mean streamwise velocity profile in inner-coordinates. The start and end of each demarcation bar in the spectra of Figure 3c is approximated as an average between the superstructure length-scale computed at the centerline of each sublayer. In this case the total contribution of the logarithmic- and outer layer structures accounts for $\approx 50\%$ of the total energy, significantly higher than the smooth-wall case where the corresponding contribution was found $\approx 30\%$ (not shown here).

To investigate the roughness impact on the fluctuating wall-shear stress, its power spectra from the three rough-wall surfaces are plotted against the corresponding one of the smooth-wall in Figure 4. Specifically, Figure 4a, which presents the PSD(τ'_w) in outer units suggests that the roughness effect on the WSS scales with the mean-roughness height. As a result, the BS39 and BR39 surfaces yield the high-

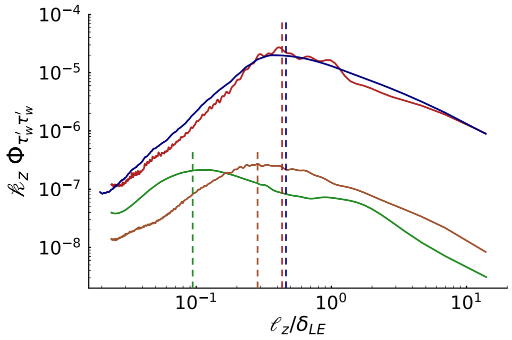

(a)

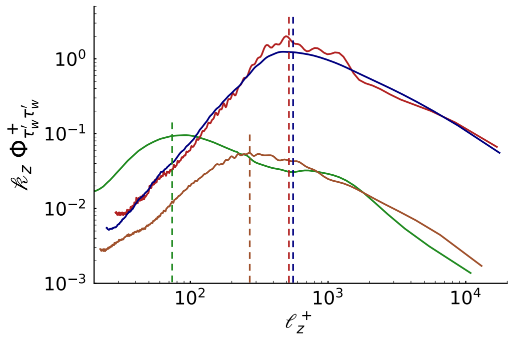

(b)

Figure 4: Premultiplied spanwise power spectra of the fluctuating wall-shear stress, τ'_w in (a) inner- and (b) outer-scaling for all surface cases at the streamwise location of $x/\delta_{LE} = 57.5$; Spectra are averaged in time and space; —— Smooth-wall; —— BS39; —— BR39; —— TR39. Dashed lines indicate the roughness length-scales obtained from the surface ray-tracing, and the superstructure width at the viscous sublayer (smooth-wall).

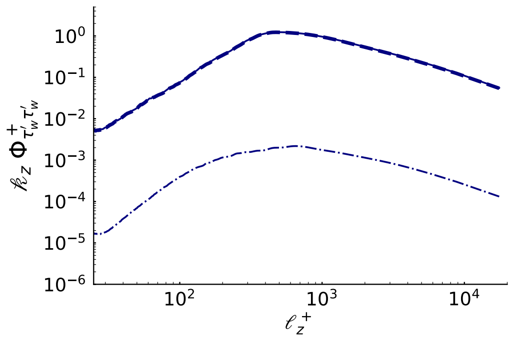

(a)

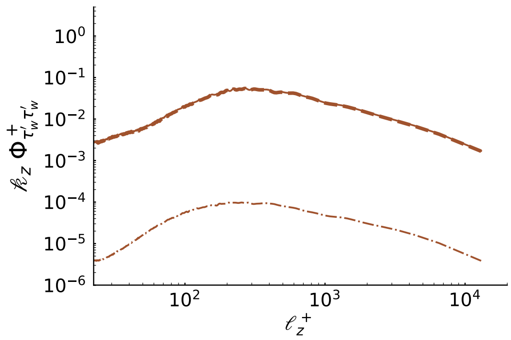

(b)

Figure 5: Premultiplied spanwise power spectra of the fluctuating wall-shear stress, τ'_w in the case of the (a) BR39 and (b) the TR39 surface cases at the streamwise location of $x/\delta_{LE} = 57.5$ in inner-coordinates; Spectra are averaged in time and space; —— Total wall-shear stress, τ'_w; - - - Pressure wall-shear stress, $\tau'_{w,pressure}$; —·— Viscous wall-shear stress, $\tau'_{w,viscous}$.

est power spectral energy, with the TR39 surface following. It is noteworthy that the PSD(τ'_w) peak of the TR39 surface is barely above the corresponding one of the smooth-wall, despite the fact that the equivalent peak in the power spectra of the pressure fluctuations is significantly above the one of the smooth-wall (not show here for brevity). This is attributed to the complex three-dimensional shape of the tubeworm-type organisms relative to the streamwise direction, to which the wall-shear stress is computed. In addition, Figure 4a suggests that there is a clear shift of the spectra peak towards larger wavelengths. Specifically, the PSD peaks correspond to the streamwise-average spanwise characteristic length-scale of each topography, as extracted from ray-tracing the surface height map. These length-scales are shown in Figure 4 in dashed lines. Interestingly, the latter observation suggests that the PSD(τ'_w) peak in such turbulent flows is geometrically induced. In the case of the smooth-wall, the peak of the PSD corresponds to the superstructure width at the center of the viscous sublayer, as captured in Kaminaris *et al.* (2025*a*). On the other hand, when the power spectra are scaled in inner-units the TR39 PSD(τ'_w) peak is found to be lower relative to the one in the smooth-wall, as shown in Figure 4b, while still corresponding to a much larger wavelength. Overall, the preceding analysis suggests that the presence of roughness obliterates essentially all the canonical smooth-wall dynamics on a spectral basis.

The pressure and viscous contribution to the total wall-shear stress power spectra is shown in Figure 5 for the BR39 and TR39 surfaces. Figure 5 indicates that the PSD(τ'_w) derived from pressure force fluctuations accounts for virtually all of the wall-shear stress energy, and it is at least three orders of magnitude larger compared to the viscous-based PSD(τ'_w). For the same test surfaces the mean form drag had been found to account for ≈90% of the mean total drag; however, the form drag contribution appears to increase further in the case of the fluctuating flow field. Furthermore, the dominance of the fluctuating form drag seems to also be independent of the mean-roughness height, as suggested by Figure 5b, for the case of the lower height TR39 topography.

Conclusions

This study presents a spectral analysis of the fluctuating wall-shear stress in turbulent boundary layers over irregular rough-walls at significant Reynolds numbers. Given the spatiotemporal coherence of superstructures—which extend from the boundary layer edge down to the wall—we demonstrate that the wall-shear stress energy spectrum reflects the length-scales of these outer-layer features. Notably, the integrated energy associated with these scales can account for up to half of the total spectral energy. In addition, it is concluded that the spectrum energy of the wall-shear stress seems to scale with the mean-roughness height, while its peak is found to correlate with the spanwise characteristic length-scale, which is estimated through ray-tracing the surfaces in the spanwise direction. Lastly, it is found the power spectral energy of the τ_w' based on the pressure force fluctuations accounts for virtually all of the total wall-shear stress energy in all of the surfaces investigated.

REFERENCES

Chung, Daniel, Hutchins, Nicholas, Schultz, Michael P. & Flack, Karen A. 2021 Predicting the drag of rough surfaces. *Annual Review of Fluid Mechanics* **53** (1), 439–471.

Hutchins, N. & Marusic, Ivan 2007 Evidence of very long meandering features in the logarithmic region of turbulent boundary layers. *Journal of Fluid Mechanics* **579**, 1–28.

Jiménez, J. 2004 Turbulent flows over rough walls. *Annual Review of Fluid Mechanics* **36** (1), 173–196.

Kaminaris, Ioannis K., Balaras, Elias & Schultz, Michael Paul 2025*a* The spatio-temporal evolution of superstructures over rough-wall turbulent boundary layers. *Journal of Fluid Mechanics* **1021**, A25.

Kaminaris, Ioannis K., Balaras, Elias, Schultz, Michael P. & Volino, Ralph J. 2023 Secondary flows in turbulent boundary layers developing over truncated cone surfaces. *Journal of Fluid Mechanics* **961**, A23.

Kaminaris, Ioannis K., Balaras, Elias, Vishwanathan, Vidya & Schultz, Michael P. 2025*b* On the impact of frontal solidity on turbulent boundary layers over irregular bio-inspired surfaces. *International Journal of Heat and Fluid Flow* **117**, 109991.

Kevin, Kevin, Monty, Jason & Hutchins, Nicholas 2019 Turbulent structures in a statistically three-dimensional boundary layer. *Journal of Fluid Mechanics* **859**, 543–565.

Kim, K. C. & Adrian, R. J. 1999 Very large-scale motion in the outer layer. *Physics of Fluids* **11** (2), 417–422.

Marusic, I., Chandran, D., Rouhi, A, Fu, M, Wine, D, Holloway, B, Chung, D & Smits, A.J. 2021 An energy-efficient pathway to turbulent drag reduction. *Nat Commun* **12**, 5805.

Marusic, I., Mathis, R. & Hutchins, N. 2010 Predictive model for wall-bounded turbulent flow. *Science* **329** (5988), 193–196.

Schultz, MP, Bendick, JA, Holm, ER & Hertel, WM 2011 Economic impact of biofouling on a naval surface ship. *Biofouling* **27** (1), 87—98.

Sillero, Juan A., Jiménez, Javier & Moser, Robert D. 2014 Two-point statistics for turbulent boundary layers and channels at Reynolds numbers up to $\delta^+ \approx 2000$. *Physics of Fluids* **26** (10), 105109.

Wu, Y. & Christensen, K. T. 2010 Spatial structure of a turbulent boundary layer with irregular surface roughness. *Journal of Fluid Mechanics* **655**, 380–418.

Yang, Jianming & Balaras, Elias 2006 An embedded-boundary formulation for large-eddy simulation of turbulent flows interacting with moving boundaries. *J. Comput. Phys* **215** (1), 12–40.

Örlü, Ramis & Schlatter, Philipp 2011 On the fluctuating wall-shear stress in zero pressure-gradient turbulent boundary layer flows. *Physics of Fluids* **23** (2), 021704.